Supplementary Information: Investigation of the $Cs_2(Mo,Te)O_4$ solid solution and implications on the Joint Oxyde-Gaine system in Fast Neutron Reactors

Enrica Epifano,[†] Andrea Volfi,[‡] Maas Abbink,[†] Hendrik Nieuwland,[†] Lambert van Eijck,[†] Gilles Wallez,[¶,§] Dipanjan Banerjee,[‖] Philippe M. Martin,[⊥] and Anna L. Smith[*,†]

†*Delft University of Technology, Faculty of Applied Sciences, Radiation Science and Technology Department, Mekelweg 15, 2629 JB Delft, The Netherlands*

‡*Politecnico di Milano, Department of Energy, Nuclear Engineering Division, Via La Masa 34, 20156 Milano, Italy*

¶*Chimie ParisTech, PSL University, CNRS, Institut de Recherche de Chimie Paris, 75005 Paris, France*

§*UFR 926, Sorbonne Université, 75005 Paris, France*

‖*Department of Chemistry, KU Leuven, Celestijnenlaan 200F, bus 2404, 30001 Leuven, Belgium.*

⊥*CEA, DES, ISEC, DMRC, Univ Montpellier, Marcoule, France*

E-mail: a.l.smith@tudelft.nl

1 Supplementary crystallographic data

1.1 Neutron diffraction data $Cs_2Mo_{0.5}Te_{0.5}O_4$

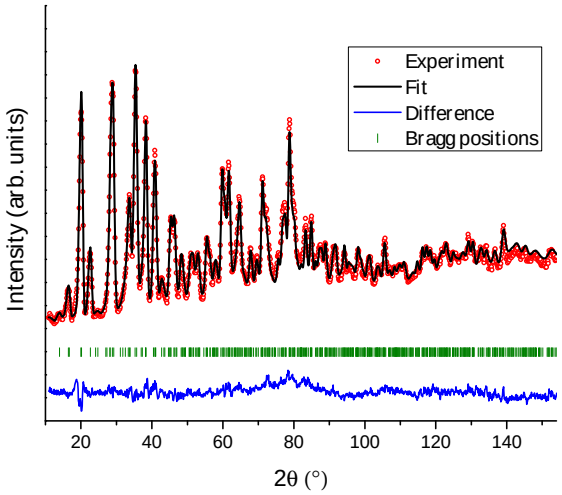

Figure S1: Experimental (red dots) and calculated (black line) neutron diffraction pattern of $Cs_2Mo_{0.5}Te_{0.5}O_4$. The background was taken as linear interpolation between operator-selected points in the pattern with refinable heights. Goodness of fit parameters are : R_{wp} = 11.6, R_p = 13.4, χ^2 = 5.33.

1.2 Anisotropic atomic displacement factors

- B^*_{eq} (Å^2) for Cs_2TeO_4:

  Cs1: B_{11}=3.5(4), B_{22}=3.7(4), B_{33}=2.6(3), B_{13}=-0.3(4)

  Cs2: B_{11}=3.3(5), B_{22}=3.2(4), B_{33}=2.2(4), B_{13}=-0.4(3)

  Te: B_{11}=2.3(4), B_{22}=2.1(3), B_{33}=2.4(3), B_{13}=-0.2(4)

  O1: B_{11}=6.5(6), B_{22}=9.6(7), B_{33}=1.0(3), B_{13}=0.1(5)

  O2: B_{11}=2.1(4), B_{22}=5.1(5), B_{33}=4.1(5), B_{13}=-1.3(4)

  O3: B_{11}=4.5(3), B_{22}=2.8(3), B_{33}=6.7(4), B_{13}=-1.6(2), B_{13}=2.2(4), B_{13}=0.1(3)

- B^*_{eq} (Å^2) for $Cs_2Mo_{0.5}Te_{0.5}O_4$:

  Cs1: B_{11}=3.0(4), B_{22}=3.6(4), B_{33}=2.5(3), B_{13}=-0.5(4)

  Cs2: B_{11}=2.3(4), B_{22}=3.0(4), B_{33}=1.8(4), B_{13}=-0.2(3)

  Te/Mo: B_{11}=2.0(4), B_{22}=2.4(3), B_{33}=1.6(3), B_{13}=-0.1(3)

  O1: B_{11}=5.2(4), B_{22}=8.7(6), B_{33}=0.6(3), B_{13}=-0.2(4)

  O2: B_{11}=2.4(4), B_{22}=5.4(5), B_{33}=3.7(5), B_{13}=-1.4(4)

  O3: B_{11}=3.7(3), B_{22}=3.1(3), B_{33}=5.4(4), B_{13}=-1.3(2), B_{13}=1.6(3), B_{13}=0.1(3)

1.3 EXAFS data fitted at the Mo K-edge.

All the structural parameters resulting from the EXAFS fit are shown in Table S1. The Debye-Waller factors σ^2 are also shown. It is important to remember that the EXAFS Debye-Waller factor differs from that of XRD and ND. In XRD and ND, the Debye-Waller factor originates from the vibration of an atom around its equilibrium position. In EXAFS, the Debye-Waller factor is due to the mean-square relative displacement of absorber and backscatterer atoms.[1,2] This implies that, despite the thermal agitation, σ^2 can be very small if the probed atom and the backscatterer neighbour move in the same way. For this

Table S1: Results of the EXAFS fit (Mo K-edge). N is the number of atoms in the coordination shell, σ^2 is the Debye-Waller coefficient and R^2 the goodness-of-fit.

Sample	Shell	distance (Å)	N	σ^2 (Å^2)	R^2
Cs_2MoO_4	O	1.78(1)	3.9(5)	0.0016(5)	0.007
	Cs	3.89(2)	4.7(8)	0.019(1)	
$Cs_2Mo_{0.95}Te_{0.05}O_4$	O	1.78(1)	3.9(8)	0.0016(6)	0.008
	Cs	3.90(2)	4.5(8)	0.019(1)	
$Cs_2Mo_{0.90}Te_{0.10}O_4$	O	1.78(1)	3.9(8)	0.0016(6)	0.008
	Cs	3.90(2)	4.8(8)	0.020(1)	
$Cs_2Mo_{0.50}Te_{0.50}O_4$	O	1.78(1)	3.9(8)	0.0016(5)	0.008
	Cs	3.91(2)	4.3(8)	0.019(1)	
$Cs_2Mo_{0.20}Te_{0.80}O_4$	O	1.78(1)	3.7(8)	0.0015(5)	0.007
	Cs	3.91(2)	4.2(6)	0.019(1)	

reason, the difference between the EXAFS σ^2 and the ND B_{eq} values does not represent an inconsistency.

The σ^2 values associated to the Cs neighbouring shell are one order of magnitude higher than those of the first oxygen shell. This is one of the causes of the low intensity of the Fourier Transform (FT) peak associated to the Mo-Cs path (the peak around 3 Å). Another important factor is the destructive interference between the contribution of the Mo-Cs and Mo-O-Mo paths to the EXAFS spectrum. This is clearly visible when observing the calculated $\chi(k)$ associated to each path, as shown for Cs_2MoO_4 in Fig. S2. It can be noticed that the $\chi(K)$ contributions of the Mo-Cs and Mo-O-Mo-O paths have comparable intensity and they interfere destructively over a wide k range.

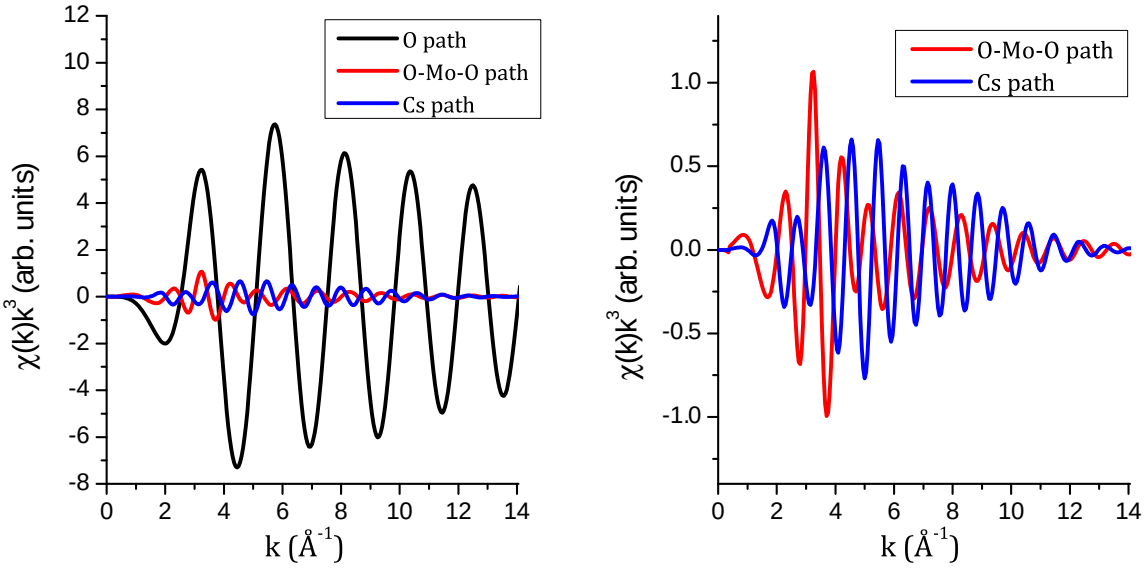

Figure S2: Calculated EXAFS signals at the Mo K-edge of Cs_2MoO_4.

1.4 Fourier difference map β-Cs_2TeO_4

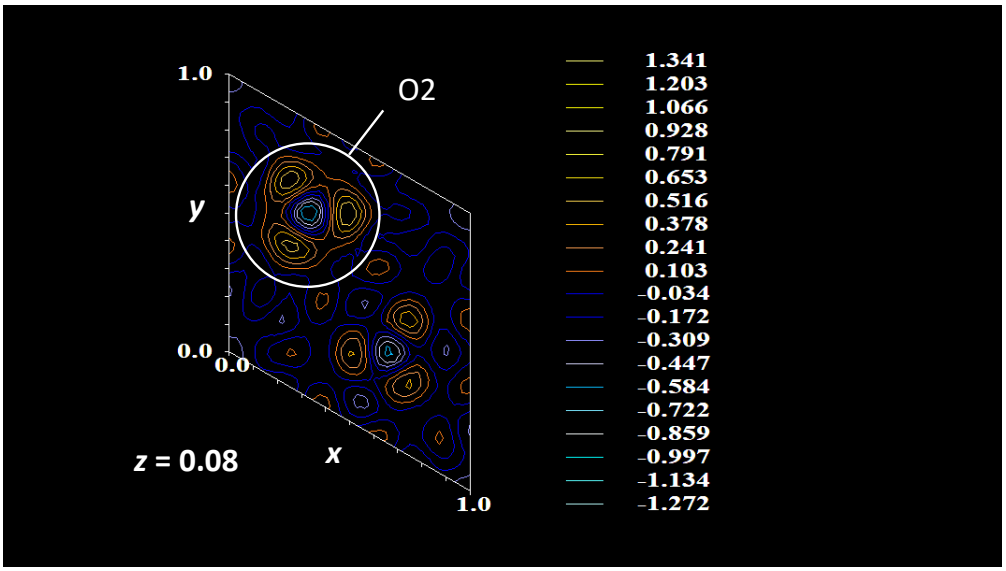

Figure S3: Fourier-difference map of the z = 0.08 plane showing the splitting of the apical O2 atom, obtained from the X-ray diffraction pattern collected at T = 773 K on the hexagonal β-Cs_2TeO_4 structure.

2 Transition enthalpy determination

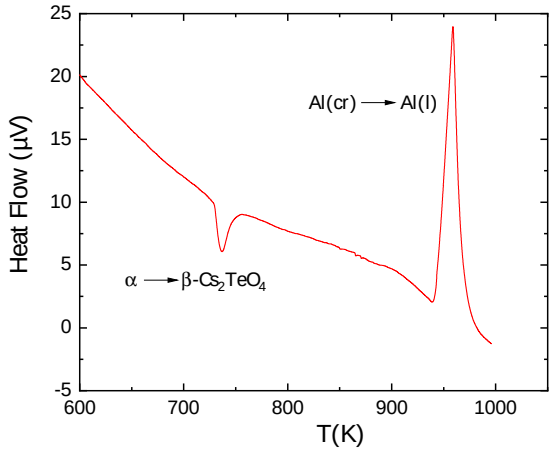

Figure S4: Heat flow curve for Cs_2TeO_4 measured against an Al reference.

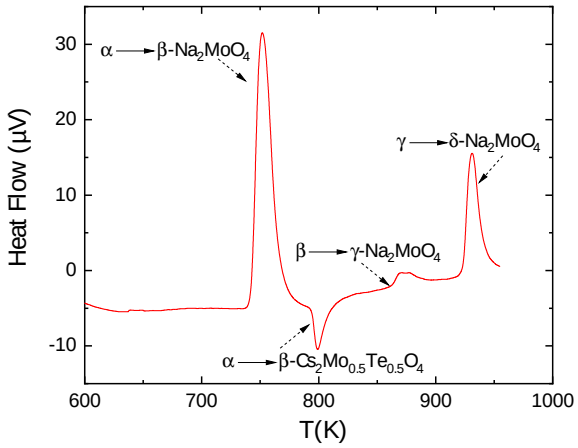

Figure S5: Heat flow curve for $Cs_2Mo_{0.5}Te_{0.5}O_4$ measured against a Na_2MoO_4 reference.

3 Regular solution model of the Cs_2MoO_4-Cs_2TeO_4 system

The development of a thermodynamic model for the Cs_2MoO_4-Cs_2TeO_4 system using a regular solution model requires to define the Gibbs energy functions of the Cs_2MoO_4 and Cs_2TeO_4 end-members, both in the solid and liqud states. A number of studies have been reported on Cs_2MoO_4 and its thermodynamic properties are well-known. The standard enthalpy of formation at 298.15 K was taken from Smith et al.,[3] the standard entropy at 298.15 K from the review by Cordfunke and Konings,[4] and the heat capacity at high temperatures from the TAF-ID database.[5] The transition and fusion enthalpies were selected from Cordfunke and Konings,[4] while the transition and melting temperatures were taken from the measured data in this work. The heat capacity of liquid Cs_2MoO_4 selected in the review of Cordfunke and Konings[4] was retained.

By contrast, the available thermodynamic data on Cs_2TeO_4 are much more limited. The standard enthalpy of formation at 298.15 K has been measured by Cordfunke et al. using solution calorimetry,[6] yielding $-(1119.5 \pm 4.6)$ kJ·mol^{-1} as recommended in the review by Cordfunke and Konings.[4] The low temperature heat capacity has not been measured to this date, and only an estimated value of the standard entropy at 298.15 K has been reported, i.e. (233 ± 5) J·K^{-1}mol^{-1}.[4] Enthalpy increment data have been measured in the temperature range (298 to 744 K) by Cordfunke et al.,[4] but were never published. Only the fitted enthalpy increment function is reported in the review by Cordfunke and Konings.[4] The latter equation yields $C_{p,m}(Cs_2TeO_4)$ = (108.7459 + 0.13283 T) J·K^{-1}mol^{-1} in the range (298-744 K). When comparing this function with that of Cs_2MoO_4, it is clear that the extrapolation beyond $\sim$ 600 K most probably leads to overestimated values. The difference between the heat capacity of Cs_2TeO_4[4] and Cs_2MoO_4[5] is around 3 J·K^{-1}mol^{-1} up to 500 K. For the present model, we assume that this 3 J·K^{-1}mol^{-1} difference is kept up to the melting temperature of Cs_2TeO_4, and propose to approximate the heat capacity at

high temperature with the following equation:

$$C_{p,m}(Cs_2TeO_4, cr) = 98.9182 + 0.18822(T/K) - 95472(T/K)^{-2} - 7.031410^{-5}(T/K)^2 \quad (1)$$

The latter function is shown in Figure S6a, where it is compared with the data reported by Cordfunke and Konings,[4] and two Neumann-Kopp approximations of the heat capacity applied to Cs_2O[7] and TeO_3,[8] and to Cs_2O[9] and TeO_3,[8] respectively. The proposed equation is in good agreement with the equation of Cordfunke and Konings[4] up to 500 K, and gives a heat capacity value at the melting point (1187.4 K) around the average value of the two Neumann-Kopp approximations. Moreover, the corresponding enthalpy increment in the range (298 to 744 K) follows very closely the equation selected in the review by Cordfunke and Konings.[4]

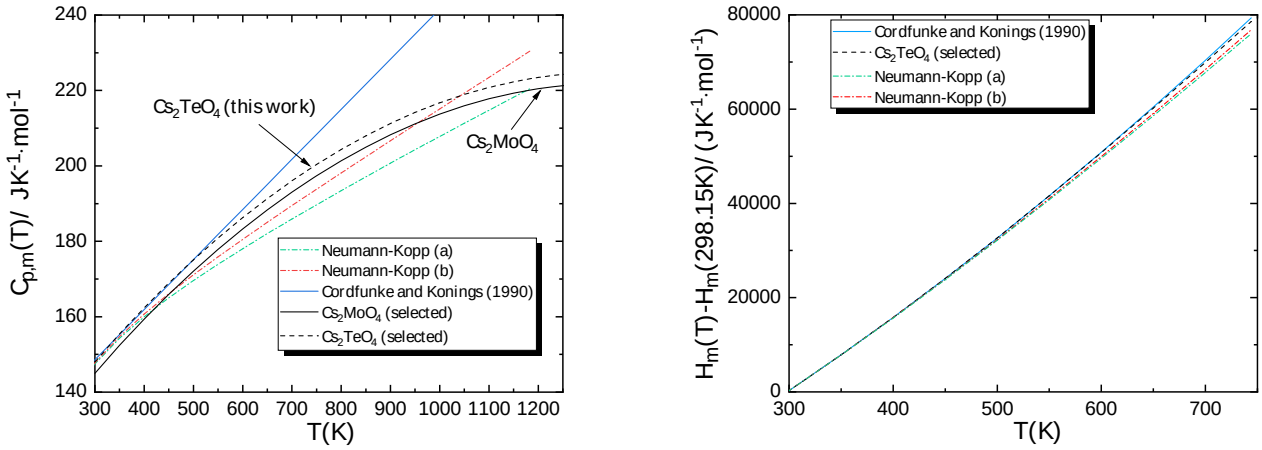

(a) $C_{p,m}(T)$ (b) $H_m(T)$-$H_m(298K)$

Figure S6: (a) Heat capacity functions for Cs_2MoO_4 and Cs_2TeO_4. (b) Enthalpy increment functions for Cs_2TeO_4. The dotted line corresponds to the selected function for the thermodynamic model. The equation reported in the review by Cordfunke and Konings[4] is shown in blue. Approximations of the heat capacity using the Neumann-Kopp rule applied to (a) Cs_2O[7] and TeO_3,[8] and (b) Cs_2O[9] and TeO_3[8] are also shown as red and green dotted lines.

Finally, two more assumptions had to be made to construct a thermodynamic model.

The first one is the enthalpy of melting of Cs_2TeO_4, which was never measured to this date. We have assumed that the entropies of fusion of Cs_2TeO_4 and Cs_2MoO_4 were equal, i.e. 25.94 $J{\cdot}K^{-1}{\cdot}mol^{-1}$. The corresponding enthalpy of fusion for Cs_2TeO_4 at 1187.4 K yields 30.8 $kJ{\cdot}mol^{-1}$. Finally, the heat capacity of liquid Cs_2TeO_4 is unknown. The same value as for Cs_2MoO_4 (i.e. 210.154 $J{\cdot}K^{-1}{\cdot}mol^{-1}$) was adopted for the present model. It is clear that a more accurate model can be developed once experimental information on the cesium tellurate becomes available.

Table S2: Summary of thermodynamic data selected in the present work.

Phase	$\Delta_f H^o_m$(298.15K)/ ($kJ{\cdot}mol^{-1}$)	S^o_m(298.15K)/ ($J{\cdot}K{\cdot}mol^{-1}$)	$\Delta_{tr} H^o_m$ ($kJ{\cdot}mol^{-1}$)	T_{tr}/(K)	Ref.
Cs_2MoO_4(α,cr)	-1514.7 $\pm$ 1.5	248.35 $\pm$ 0.30	4.6 $\pm$ 0.8	839.1 $\pm$ 5	[3,4] This work
Cs_2MoO_4(β,cr)			31.8 $\pm$ 0.8	1225.7 $\pm$ 5	[4] This work
Cs_2TeO_4(α,cr)	-1119.5 $\pm$ 4.6	233 $\pm$ 5	2.67 $\pm$ 0.14	712.3 $\pm$ 5	[4] This work
Cs_2TeO_4(β,cr)			30.8	1187.4 $\pm$ 5	This work

Table S3: Summary of heat capacity data selected in the present work.

Phase	$C_{p,m}$=A+B·T+C·T^{-2}+D·T^2/$J{\cdot}K^{-1}{\cdot}mol^{-1}$				Temp. range/K	Ref.
	A	B	C	D		
Cs_2MoO_4(cr)	95.9182	$18.82224{\cdot}10^{-2}$	−95472	$-7.0314{\cdot}10^{-5}$	298.15-1229.5	[5]
Cs_2MoO_4(l)	210.154				>1229.5	[4]
Cs_2TeO_4(cr)	98.9182	$18.82224{\cdot}10^{-2}$	−95472	$-7.0314{\cdot}10^{-5}$	298.15-1187.4	This work
Cs_2TeO_4(l)	210.154				>1187.4	This work

References

(1) Lee, P. A.; Citrin, P. H.; Eisenberger, P.; Kincaid, B. M. Extended x-ray absorption fine structure-its strengths and limitations as a structural tool. *Rev. Mod. Phys. 53*, 769–806, Publisher: American Physical Society.

(2) Dalba, G.; Fornasini, P. EXAFS Debye–Waller Factor and Thermal Vibrations of Crystals. *J. Synchrotron Radiat. 4*, 243–255.

(3) Smith, A. L.; Pignié, M.-C.; Eijck, L. V.; Griveau, J.-C.; Colineau, E.; Konings, R. J. M. Thermodynamic study of $Cs_3Na(MoO_4)_2$: Determination of the standard enthalpy of formation and standard entropy at 298.15 K. *J. Chem. Thermodynamics* **2018**, *120*, 205–2016.

(4) Cordfunke, E. H. P.; Konings, R. J. M. *Thermochemical data for reactor materials and fission products*; Thermochemical data for reactor materials and fission products, Elsevier Science Publishers B. V., 1990.

(5) *Thermodynamics of AdVanced Fuels – International Database (TAF-ID), www.oecd-nea.org/science/taf-id/)*.

(6) Cordfunke, E. H. P.; Ouweltjes, W.; Prins, G. Standard enthalpies of formation of tellurium compounds III. Cs_2TeO_3, $Cs_2Te_2O_5$, $Cs_2Te_4O_9$, and Cs_2TeO_4. *J. Chem. Thermodynamics* **1988**, *20*, 569–573.

(7) Guéneau, C.; Flèche, J.-L. Thermodynamic assessment of the cesium-oxygen system by coupling density functional theory and CALPHAD approaches. *Calphad* **2015**, *49*, 67–78.

(8) Cordfunke, E. H. P.; Cluistra, R.; Miltenburg, J. C. V. The thermodynamic properties of six compounds in (tellurium+oxygen+hydrogen) from 10 to 1000 K. *J. Chem. Thermodynamics* **1985**, *17*, 1079–1089.

(9) Dinsdale, A. T. SGTE Data for Pure Elements. *Calphad* **1991**, *15(4)*, 317–425.